SES6-CT-2004-502599

CO2SINK

In-situ R&D Laboratory for Geological Storage of CO_2

Integrated Project

Thematic Priority: 6.1.ii

Deliverable 6.1-5 Interim Progress Report Numerical Investigations on CO_2 Injection into Geological Formations

Due date of deliverable: month 17
Actual submission date: month 17

Start date of project: 01.04.04 Duration: 60 months

A. Bielinski, A. Kopp, H. Class, R. Helmig, IWS, Universität Stuttgart

Project co-funded by the European Commission within the Sixth Framework Programme (2002-2006)		
Dissemination Level		
PU	Public	
PP	Restricted to other programme participants (including the Commission Services)	
RE	Restricted to a group specified by the consortium (including the Commission Services)	
CO	Confidential, only for members of the consortium (including the Commission Services)	

Progress Report

Contents

1 Abstract

We present results from the 3D simulations of the flow modelling, relevant for the Ketzin anticline structure.

Our study showed that the CO_2 saturation increase probably occurs very fast after the start of the injection. Saturations can rise from zero to values of 50% and higher within a few days. Maximum saturations can reach up to 100 % in the close vicinity of the injection well, when incorporating temperature effects and mutual solubilities. When neglecting these effects, a maximum CO_2 saturation of 85 % is observed for a reservoir with Ketzin like characteristics. The greater the distance to the injection well, the lower is the maximum saturation and the more gradually is the rise of the CO_2 saturation over time.
The influence of the buoyancy forces scales with the permeability of the reservoir. The higher the permeability the higher is the influence of the buoyancy forces and the more likely becomes a wide spreading of the CO_2 plume underneath the caprock. For lower permeabilities (lower than approx. 100mD), CO_2 evolves more and more in a cylindrical shape away from the injection well into the reservoir. Most influencing parameters for the saturation distribution are the permeability and the residual water saturation.

Peak overpressure always occurs shortly after injection start. This is due to low relative permeabilities and still small volume of the compressible CO_2 plume. For low permeabilities with high peak overpressures, the peak is observed weeks or a few months after start of injection. Therefore, there is a high probability, that when low permeabilities are observed in Ketzin, one would have to start with a lower CO_2 injection rate. But this rate then could be increased over time when overpressure decreases. The fracture pressure for the Ketzin reservoir is estimated to be 10 bar overpressure. Assuming a constant injection of 1 $[\frac{kg}{s}]$, overpressures are lower than this fracture pressure for a permeability higher than 100 mD. Porosity has a minor effect on the overpressure, but it has on the time, when the peak overpressure is reached. A lower porosity results in a earlier occurence of the peak overpressure.

The amount of dissolved CO_2 increases very fast to 13 $[\frac{sm^3_{CO_2}}{sm^3_{brine}}]$. In our model this is due to the immediate equilibrium assumption. The dissolved CO_2 plume always has a slightly larger extent than the saturation plume.

There is little information available about the relative permeability-saturation relation and the capillary pressure-saturation relation, representative for the Ketzin reservoir.

Based on the results of this investigation, three recommendations are made:

- A hydraulic assessment of the reservoir needs to be made before CO_2 injection begins (well testing).

- The initiation of the injection regime needs careful design as it is the reservoir properties (especially permeability) that dictate and control the pressures and will drive the injection process. It should be kept in mind that even after drilling and testing considerable uncertainties remain and surface facilities need to be able to accommodate this situation.

- Parameters and relations that should be focused on in laboratory testing include permeability, porosity, residual gas and water saturations, relative permeability-saturation relation and the capillary pressure-saturation relation.

2 Introduction and Objectives

This report documents work associated with Workpackage 6.1 Hydrodynamic Modeling, and forms Deliverable 6.1-5.

The results presented here provide valuable insights for the discussion on setting up the monitoring and verification of injected CO_2 for the CO2SINK project. The focus is, to get a sound understanding of the influence of the forces driving the system and the parameters characterising the reservoir. Parameters investigated include permeability, porosity, residual gas and water saturations, lambda (measure for the homogeneity of the reservoir in the Brooks & Corey relation, see section 3) and the influence of the selection of the boundary conditions of the reservoir on the modeling results. The simulations presented here will be expanded to more complex and realistic model domains and input parameters.

The evolution of reservoir pressure and CO_2 saturation due to injection of supercritical CO_2 is modeled with the numerical simulator MUFTE_UG [6]. Supercritical CO_2 is injected into radial symmetric reservoirs confined by a virtual cap-rock and an impermeable reservoir base. As initial conditions and for the outer lateral boundary, undisturbed hydrostatic pressure, zero initial CO_2 saturation and geothermal termperature distribution is assumed.

3 Conceptual Model

3.1 Capillary Pressure

Figure 1 shows a schematic capillary pressure-saturation relation used. We use the approach suggested by Brooks & Corey (1964) [?].

Experimental values of capillary pressures for CO_2-water or CO_2-brine systems are not generally determined. Due to the lack of data, we use the same parameters as obtained for the relative permeability function (cf. section 3.2).

It is necessary to assess the parameters for the capillary pressure-saturation relationships at the Ketzin site with direct or indirect measurements and taking into account approaches from literature.

The input parameters for this relation are given in table 1. The actual values for S_{wr}, S_{gr}, p_d and λ are given in the "Boundary Conditions and Parameter" section for each simulation (cf. section 4.2, 5.2, 6.2). The Brooks & Corey parameter λ describes the pore scale homogeneity of the reservoir, which influences both, the capillary pressure-saturation relation and the relative permeability relation.

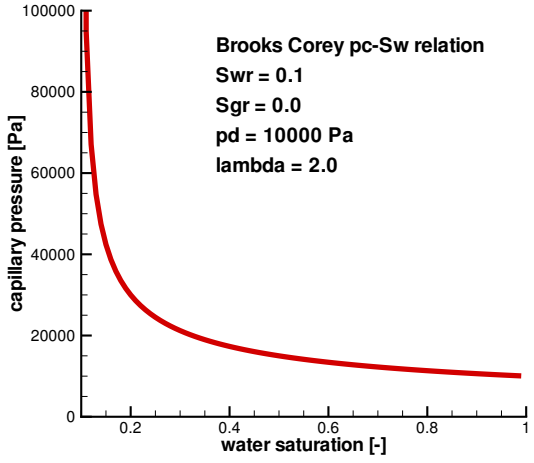

Figure 1: Capillary pressure-saturation relation.

3.2 Relative Permeability

The relative permeability-saturation relation used for the simulation is depicted in Figure 2, krw and krg are the relative permeabilities of the water and of the gas (CO_2) phase,

Table 1: Input Parameters for the Brooks & Corey capillary pressure-relation and the relative permeability function.

symbol	meaning	unit
S_{wr}	residual water saturation	[-]
S_{gr}	residual CO_2 saturation	[-]
p_d	entry pressure	[Pa]
λ	Brooks Corey parameter	[-]

respectively. The input parameters for the relative permeability relation are S_{wr}, S_{gr} and p_d and the same values are used as for the capillary pressure-saturation relation (given in the "Boundary Conditions and Parameters" section for each simulation, cf. 4.2, section 5.2, 6.2). The situation is the same as for capillary pressures, experimental determinations reported in the literature focus on the system CO_2-oil/gas for CO_2 floods to improve oil recovery and not the system CO_2-water-brine. Therefore, as a first estimate we choose a relative permeability-saturation relationship that is very similar to the one suggested by Kretzschmar et al. (1973) for the system methane - water at the Ketzin site [8, 9]. These relations have to be investigated thoroughly and adapted to the expected behaviour of CO_2 in the upcoming research.

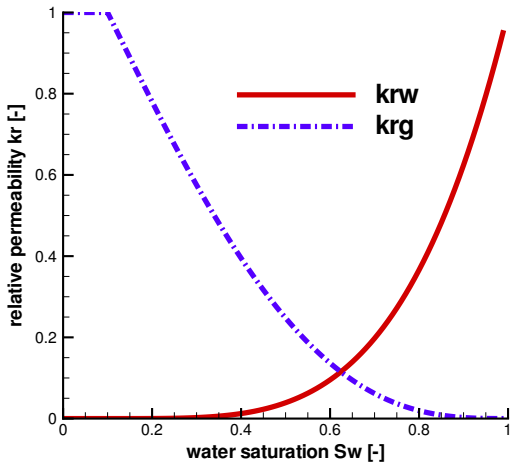

Figure 2: Relative permeability-saturation relation.

3.3 Fluid and Matrix Properties

For the Code Comparison Study (cf. section 6) the two-phase two-component non-isothermal model is used. Phases are CO_2 and brine, components are CO_2 and water. Mutual solubilities of the components as well as temperature effects are taken into account and influence the saturation and pressure evolution.

For the Parameter Study (cf. section 5) and the BaseCase Scenario (cf. section 4) a two-phase model is used. This means that we do not consider the mutual solubilities of brine and CO_2. Therefore changes in saturations can be completely attributed to the migration of the CO_2 phase in the pores of the reservoir rock. Non-isothermal effects are not taken into account. The remaining water content is determined by the residual water saturation.

Density of the brine phase depends on pressure, temperature and salinity, for the code comparison study also on the CO_2 dissolved. The density of the CO_2 phase only depends on pressure and temperature. Viscosity of the brine phase is a function of temperature and salinity. The CO_2 phase viscosity is calculated as a function of temperature, pressure and the density of CO_2.

Table 2: Fluid Properties

variable	symbol	unit
water density	ϱ_w	$[\frac{kg}{m^3}]$
water viscosity	μ_w	[Pa·s]
CO_2 density	ϱ_{CO2}	$[\frac{kg}{m^3}]$
CO_2 viscosity	μ_{CO2}	[Pa·s]

The brine of the Schilfsandstein, the target reservoir for CO_2 injection, has a salinity of 250 $[\frac{g}{L}]$ (Total Dissolved Solids) and a density of 1160 $[\frac{kg}{m^3}]$, greater than that of pure water (CO2SINK data bank). This salinity has been assumed for all the simulations. This implies that the density contrast between the two phases and the buoyancy of CO_2 is enhanced in reality compared to the present simulation.

The temperature is kept constant at 35°C in case of the Parameter Study (cf. section 5) and the BaseCase (cf. section 4) scenario.

In case of the code intercomparison study some additional heat-related definitions have to be made. The enthalpy of the brine is calculated as a function of pressure, temperature, salinity and dissolved CO_2. Enthalpy of CO_2 is according to pressure and temperature. The diffusion coefficient of CO2 in water is set to $2 \cdot 10^{-9}$ $[\frac{m^2}{s}]$. The matrix density is set to $\varrho_s = 2650.0$ $[\frac{kg}{m^3}]$ and the heat capacity of the matrix is 750.0 $[\frac{J}{kg \cdot K}]$.

4 BaseCase

In this section the so called BaseCase Scenario is described. It was developed in close cooperation with all the WP6.1 modelling group. Motivation was to estimate the minimal necessary amount of CO_2 to inject and the estimation of the arrival time of the CO_2 front at the observation wells. It gave support to the planning, positioning and the layout of the injection and the observation wells. For the positioning of the observation wells in relation to the injection well, it is important to have estimates about the arrival time of the CO_2 plume. Especially the estimates for the arrival times of the 10 [%] and 60 [%] saturation fronts are of high importance. Seismic waves detect CO_2 saturations in the order of 10 [%], whereas the other (electric) geophysical methods are sensitive to higher saturations. The permeability is taken from a geostatistical model by SCRF described in section 4.3. The injection rate is constant and brine is assumed as formation fluid.

4.1 Model Domain

The model domain (see Figure 3) is a radial symmetric domain with a lateral extent of 10 [km]. The model area described this way is about 314.2 [km^2]. The smallest grid cell length is 5 [cm], this is at the injection well in the middle of the domain where the highest velocities, pressures and saturations are observed. The grid cell length then gradually increases with radial distance to the injection well. The height of the domain is 80 [m]. The injection well diameter is 4 [inches], which corresponds to 0.1016 [m]. With this approach all the effects of a full 3D representation of the reservoir can be taken into account, but with the advantage of only solving the equations for a part of the reservoir. When assuming a lateral extent of 10 [km], influence of the lateral boundary condition on the results are of minor influence.

4.2 Boundary Conditions and Parameters

The boundary conditions used for the simulation are shown in table 3. Here, the following notation is used:

p_w	water pressure (bar)
S_{CO2}	CO_2 saturation
S_w	water saturation
q_w	water mass flux (kg/s)
q_{CO2}	CO_2 mass flux (kg/s)

Top and bottom of the model domain are no-flow boundaries, corresponding to completely impermeable cap-rock and reservoir base. Due to symmetry (radial domain), also the side

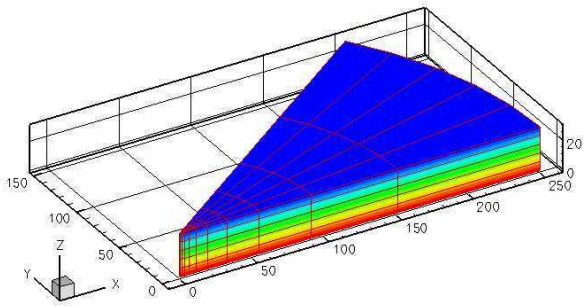

Figure 3: Inner part of a radial symmetric model domain.

boundaries have no-flow conditions. At the outer lateral boundary, hydrostatic water pressure and a constant CO_2 saturation is applied. The hydrostatic pressure refers to a depth of 680 [m] at the bottom and 600 [m] at the top of the domain.

While no flux occurs through the non screened section of the injection well, a constant CO_2 flux is forced over the inner lateral boundary (which stands for the injection well) into the model domain. This flux is fixed to 0.76 $[\frac{kg}{s}]$, which corresponds to a total mass injection of approximately 60 000 $[\frac{tons}{year}]$. CO_2 flux remains constant over the entire simulation time. The injection well is completed only in the sand channels (cf. section 4.3).

Table 3: Boundary Conditions

boundary	type	value	unit	comment
top, bottom, side	NEUMANN q_w	0.0	$\frac{kg}{m^2 \cdot s}$	NO-FLOW
top, bottom, side	NEUMANN q_{CO2}	0.0	$\frac{kg}{m^2 \cdot s}$	NO-FLOW
lateral	Dirichlet p_w	$P_{atm} + (\varrho \cdot g \cdot h)$	bar	
lateral	Dirichlet S_{CO2}	0.0	-	
injection well	NEUMANN q_w	0.0	$\frac{kg}{m^2 \cdot s}$	NO-FLOW
injection well	NEUMANN q_{CO2}	-0.76	$\frac{kg}{s}$	

For other model input parameters see table 4.

For the horizontal permeabilities and porosities see section 4.3. The domain was assumed to be non-isotropic, with a ratio of $\frac{vertical permeability}{horizontal permeability} = \frac{1}{3}$.

Table 4: Input Parameters for the BaseCase.

Parameter	type	value	unit	comment
Salinity	X	0.2	$\frac{kg}{kg}$	$= 250\ \frac{g}{L}$
Res. Water Sat.	S_{wr}	0.15	-	
Res. CO_2 Sat.	S_{nr}	0.05	-	
Entry Pressure	p_d	10000	Pa	
Lambda	λ	2	-	
Initial conditions Water	p_w	$P_{atm} + (\varrho \cdot g \cdot h)$	bar	Hydrostatic pressure
Initial conditions CO_2	S_n	0.0	bar	Saturation = 0

4.3 Geological Model

A geostatistical approach has been selected in order to describe the reservoir permeability characteristics due to the fact, that the resolution of the old seismic data available for the site does not resolve the internal architecture of the Stuttgart Formation and borehole data is sparse. The program FLUVSIM by SCRF (Deutsch & Journel (1997) [3] and Deutsch & Tran (2002) [4] has been selected to perform the geostatistical modelling. This program exploits the advantages of the hierarchical object-based modelling scheme described by (Deutsch & Wang (1996) [5]). The channel facies assumed for the Stuttgart Formation are generated as objects in a backround matrix of low permeable non-channel facies. It honours different types of secondary information as e.g. well data etc. In Figure 4 the geostatistical model is shown.

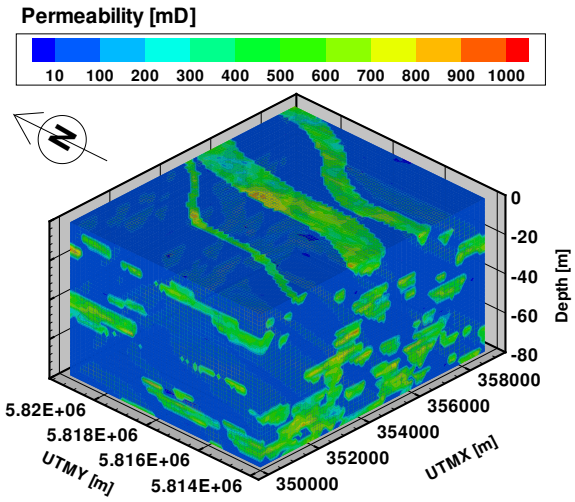

Figure 4: Geostatistical permeability distribution after FLUVSIM.

Because the emphasis is given to the near-well and short-term saturation (and pressure) evolution, only the vertical permeability distribution at the presumed drill-site (UTMX 355200,UTMY 5817900) is used as input for the flow model (see Figure 5).

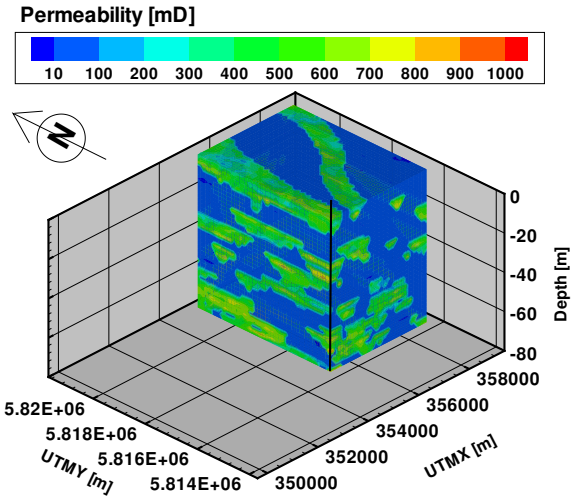

Figure 5: Geostatistical permeability distribution cut open at the presumed drill site.

The vertical permeability distribution of the FLUVSIM model at the presumed drill-site is assumed for the entire reservoir. This leads to a input permeability for the flow simulation as in figure 6. Shown is a 2D-slice of the 3D-reservoir. On the x-axis one can see the radial distance from the injection well on the left hand side (x=0). On the z-axis the depth from the bottom of the reservoir to the cap-rock is depicted. The permeability ranges from 10 [mD] for the backround matrix, up to between 368 [mD] and 705 [mD] for the channel facies. The domain was assumed to be non-isotropic, with a ratio of $\frac{vertical permeability}{horizontal permeability} = \frac{1}{3}$. The porosity is set to 17 [%] for the background matrix and 23 [%] for the channel facies.

4.4 Saturations

To get an understanding for the saturation evolution, two types of saturation plots are presented here. First, saturation evolution plots, showing the development of the saturation over time at a specific point in the reservoir. Second, saturation plots showing a vertical 2D slice of the reservoir. This plot is important to get an understanding of the influence of the layered permeability distribution on the model. Figures 7 and 8 show the saturation evolution for the injection well and the observation wells.

It can be seen that the larger the distance to the injection well, the later is the arrival of the saturation front, the lower is the maximum saturation and the more gradually is the rise of the CO_2 saturation over time. The maximum saturation is around 80 [%], this saturation

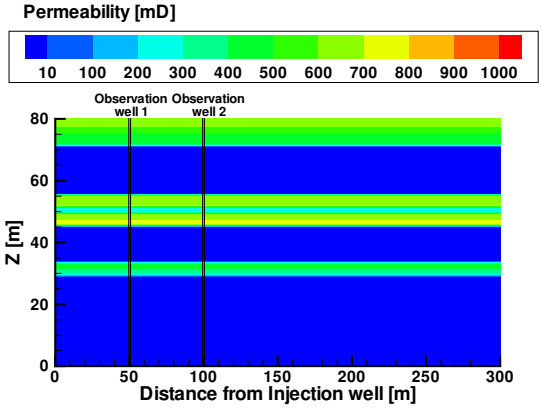

Figure 6: Permeability distribution assumed in the flow model.

is observed at the injection well after 180 days of continuous injection. From this plots, the arrival times of the 10 [%] respectively 60 [%] CO_2 saturation front can be derived. These arrival times together with the injected mass at that time and the volume are given in Table 5.

At these points in time, shown in table 5 (except for OW3) 2D-slices of the saturation distribution are shown in figure 9. Again, on the x-axis one can see the radial distance from the injection well on the left hand side (x=0) and the z-axis shows the depth from the bottom of the reservoir to the cap-rock.

Buoyancy effects are very strong, leading to a significant upwelling of CO_2 within the channel structure. But the intervening background matrix layers with low permeability in between the channels acts as a caprock itself, virtually no CO_2 is able to infiltrate into the low permeability matrix. Even at the injection well, no CO_2 rises from a lower channel to a higher one. Higher saturations than 65 [%] are only observed in the uppermost region of the sand channels. The reason for the faster plume evolution in the sand channel just underneath the caprock (between 72 [m] and 80 [m]) in comparison to the others is, that this sand channel is large and has a high permeability (see figure 6). The other sand channels are either thin (sand channel between 29 [m] and 34 [m]) or have low permeability regions within the sand channel (sand channel between 35 [m] and 56 [m]). Therefore, in the uppermost sand channel the CO_2 can rise rapidly to the caprock and there is enough CO_2 supply that drives the plume evolution. This guarantees a fast spreading of the CO_2.

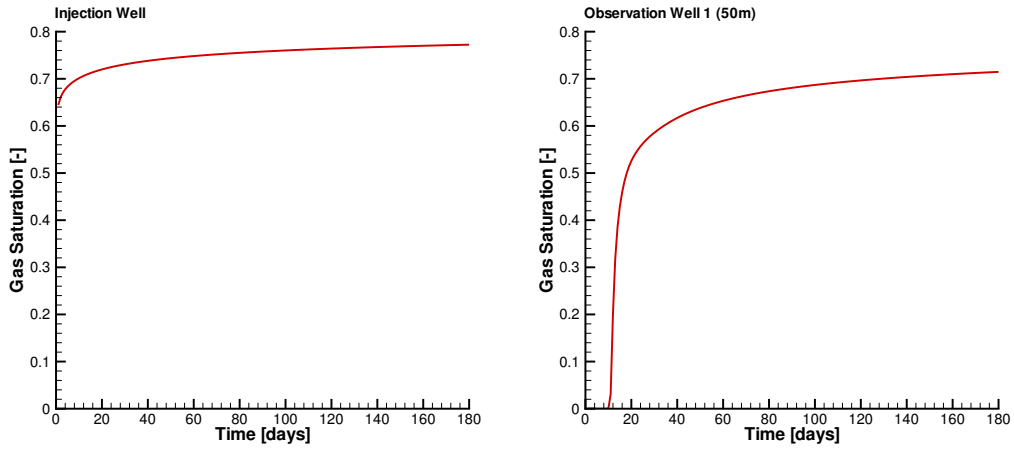

Figure 7: Saturation evolution at the cap-rock at the injection well (left) and at the observation well 1 in 50 [m] distance.

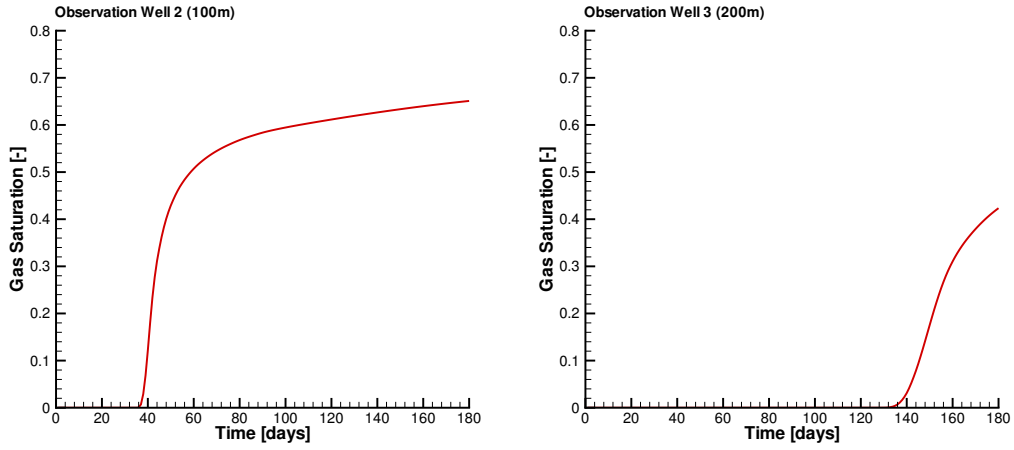

Figure 8: Saturation evolution at the cap-rock at observation well 2 (left) in 100m distance and at the observation well 3 in 200 [m] distance.

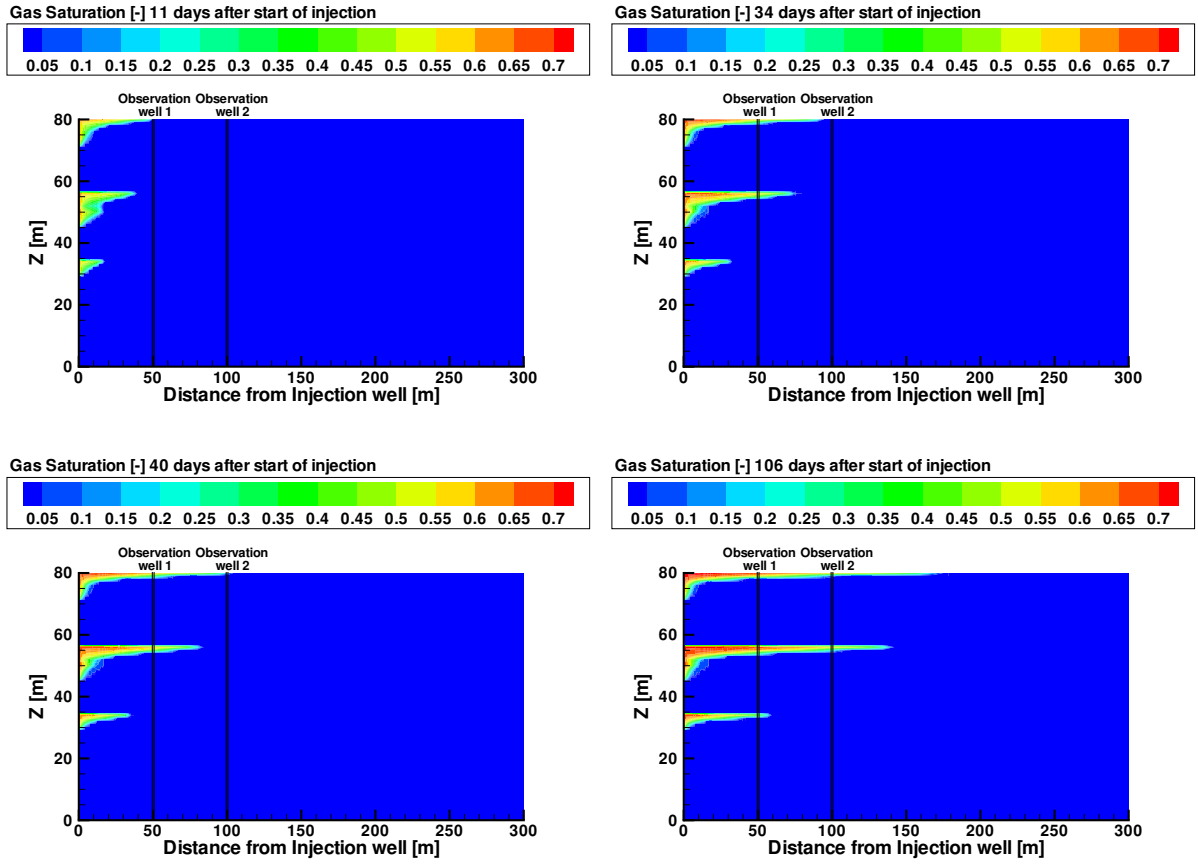

Figure 9:
Top: Saturation distribution in the reservoir when the 10 [%] saturation front reaches observation well 1 at 11 days (left) and when the 60 [%] saturation front arrives at 34 days (right) after start of injection.
Bottom: Saturation distribution in the reservoir when the 10 [%] saturation front reaches observation well 2 at 40 days (left) and when the 60 [%] saturation front arrives at 106 days (right) after start of injection.

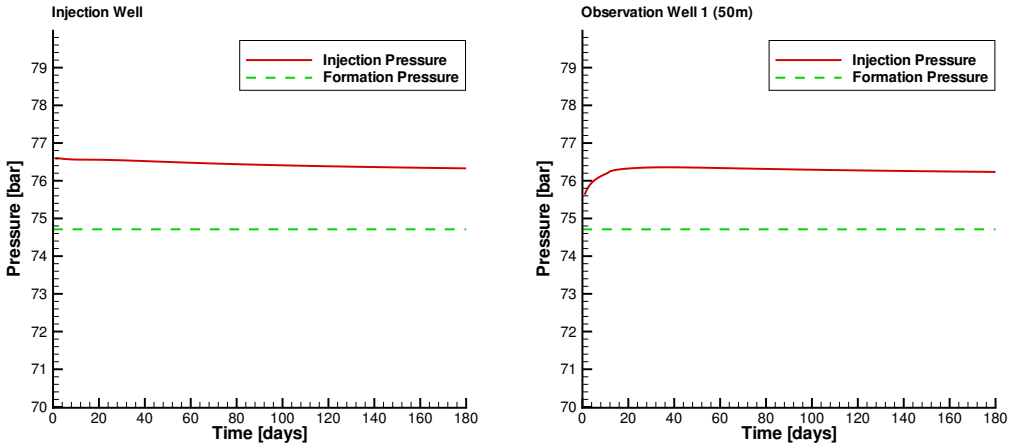

Figure 10: Pressure evolution at the cap-rock at the injection well (left) and at the observation well 1 in 50 [m] distance. The black dashed line represents the formation pressure.

4.5 Pressure Evolution

The pressure evolution in this case is of minor interest since the flux of the injected mass is lower than in the preceding cases (here 0.76 $[\frac{kg}{s}]$) and the flux is constant, whereas during the injection phase the flux could be lowered to reduce the overpressure. Figures 10 and 11 show the pressure evolution for different points in the reservoir. The formation pressure in this case is 74.7 [bar] at the cap-rock in 600 [m] depth (visualised by the green dotted line).

The maximum overpressure for this setup is 1.9 [bar]. This overpressure is observed at the cap-rock, just above the injection well, at the very beginning of the injection. It declines then continuously. For observation well 1, the maximum overpressure is slightly less. The pressure rises for 40 days, then it starts to decline. With growing distance to the injection well, the maximum overpressure is smaller and later in time. For observation well 2 the maximum overpressure is observed after about 50 days (1.5 [bar]), at observation well 3 after about 150 days (1.4 [bar]).

4.6 Arrival times, injected mass and volumes

The arrival times of the 10 [%] and 60 [%] saturation front have been derived at the observation wells for the above mentioned reasons. In the planning phase for the positions of the observation wells in relation to the injection well, it is important to have estimates about the front propagation velocity. There needs to be enough space between the injection well and the observation wells to have a big enough timespan to monitor. On the other hand there is an upper limit for the spacing between the wells due to the measurement technique and the available space at the construction site. Moreover, the injected mass has an influence on the ease to detect the plume. A larger mass is better to detect. The volume corresponding to the

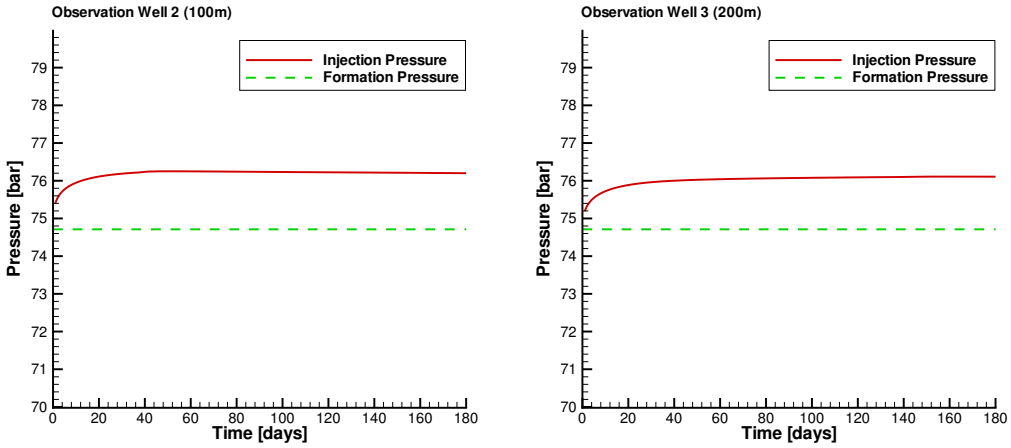

Figure 11: Pressure evolution at the cap-rock at the observation well 1 (left) in 100m distance and at observation well 3 in 200 [m] distance. The black dashed line represents the formation pressure.

given masses are calculated with the assumption of an average density of 236,1 $[\frac{kg}{m^3}]$. This corresponds to a density at 40 [°C] and 75 [bar]. With respect to the small overpressures this is appropriate. The arrival times (T), injected Mass (M) and the corresponding volume (V) are given in Table 5. The arrival time for the 60 [%] saturation front at observation well 3 is missing because the model was stopped before.

Table 5: Arrival times (T), injected Mass (M) in [tons] and corresponding volume (V) for the 10 [%] and the 60 [%] saturation front at the observation wells (OW1 at 50 [m], OW2 at 100 [m], OW3 at 200 [m] radial distance to injection well).

S_n	OW_1			OW_2			OW_3		
[%]	T[days]	M[to]	V[m^3]	T[days]	M[to]	V[m^3]	T[days]	M[to]	V[m^3]
10	11,4	748,6	3,23	39,6	2.600,3	11,23	145,5	9.554,1	41,25
60	34,1	2.239,1	9,67	106,0	6.960,4	30,05	-	-	-

The 10 [%] saturation front reaches the first observation well after 11,4 [days], this time can even be shorter in reality when taking into account the possibility, that the injection well and the first observation well are connected by a sand channel with a higher permeability, though this is unlikely. In this model setup a total CO_2 mass of 10 000 [tons] would be sufficient to be able to detect a 10 [%] CO_2 saturation at an observation well in 200m distance.

5 Parameter Study

With this Parameter Study the issue of parameter uncertainty is addressed. The information about the parameters for the Stuttgart Formation in Ketzin were very sparse in the beginning of the project. Furthermore, the coupled equation system used to describe the multiphase flow regime of CO_2 injection into the subsurface, is highly nonlinear and the influence of a single parameter difficult to predict. Therefore it is important to get a sound understanding of the influence and the interaction of the input parameters of the equation system to the modelling process of CO_2 sequestration. We set up a Ketzin like scenario with expected parameter values. Starting from this parameter values, we varied the most important parameters and compared the result of pressure evolution and saturation distribution with the original case. As parameters to investigate have been identified: Radial extent of the model domain, absolute permeability, porosity, residual water saturation, residual gas saturation and λ (λ describes the pore scale homogeneity of the reservoir, which influences the capillary pressure - saturation relation and the relative permeability relation, cf. section 3). See Table 6 for names and values of the variations.

Table 6: Parameter Variations used in the Parameter Study.

Case-Name	Radial Extent of Domain	Permeability	Porosity	Residual Water Sat.	Residual Gas Sat.	λ
	[m]	[m^2]	[-]	[-]	[-]	[-]
RAD0	**5000**	$\mathbf{10^{-13}}$	**0.2**	**0.1**	**0.05**	**2**
RAD1	**500**	10^{-13}	0.2	0.1	0.05	2
RAD2	**1000**	10^{-13}	0.2	0.1	0.05	2
PERM1	5000	$\mathbf{10^{-12}}$	0.2	0.1	0.05	2
PERM2	5000	$\mathbf{10^{-14}}$	0.2	0.1	0.05	2
PORO1	5000	10^{-13}	**0.15**	0.1	0.05	2
PORO2	5000	10^{-13}	**0.25**	0.1	0.05	2
SWR1	5000	10^{-13}	0.2	**0.4**	0.05	2
SWR2	5000	10^{-13}	0.2	**0.0**	0.05	2
SNR1	5000	10^{-13}	0.2	0.1	**0.0**	2
SNR2	5000	10^{-13}	0.2	0.1	**0.2**	2
LAMBDA1	5000	10^{-13}	0.2	0.1	0.05	**1.5**
LAMBDA2	5000	10^{-13}	0.2	0.1	0.05	**3**

5.1 Model Domain

The model domain is the same as for the BaseCase scenario (see Figure 3) but with different dimensions. The radial symmetric domain now has a lateral extent of 5 [km] (for the case which is the basis for all the parameter variations (named RAD0)). Two variations from that have been modelled with a lateral extent of 500 [m] (named RAD1) and 1000 [m] (named RAD2). The modelarea described is about 78.5 [km^2] (RAD0). The smallest grid cell length is 20 [cm] at the injection well. The height of the domain is 30 [m] and the injection well diameter is 0.14 [m]. The domain was assumed to be isotropic.

5.2 Boundary Conditions and Parameters

The boundary conditions used are the same as in the BaseCase scenario, but with a different injection rate and different well completion (see Table 7). The well is completed in the lowest section of the reservoir over a length of 5 [m]. A constant CO_2 flux is forced over this boundary into the model domain with a fixed rate of 1 [$\frac{kg}{s}$]. CO_2 flux remains constant over the entire simulation time. The hydrostatic pressure refers to a depth of 760 [m] at the bottom and 730 [m] at the top of the domain. This is to ensure supercritical conditions.

Table 7: Boundary Conditions

boundary	type	value	unit	comment
top, bottom, side	NEUMANN q_w	0.0	$\frac{kg}{m^2 \cdot s}$	NO-FLOW
top, bottom, side	NEUMANN q_{CO2}	0.0	$\frac{kg}{m^2 \cdot s}$	NO-FLOW
lateral	Dirichlet p_w	$P_{atm} + (\varrho \cdot g \cdot h)$	bar	
lateral	Dirichlet S_{CO2}	0.0	-	
injection well	NEUMANN q_w	0.0	$\frac{kg}{m^2 \cdot s}$	NO-FLOW
injection well	NEUMANN q_{CO2}	-1.0	$\frac{kg}{s}$	

Other input parameters used to describe the system, besides the already defined variation parameters can be seen in table 8.

5.3 Saturations

The saturation evolution is shown for different distances to the injection well and for different points in time (see figure 12).

The RAD0-Case is the basis for all the interpretations and is described as follows:
The saturation one week after injection start in 5 [m] distance to the injection well reaches

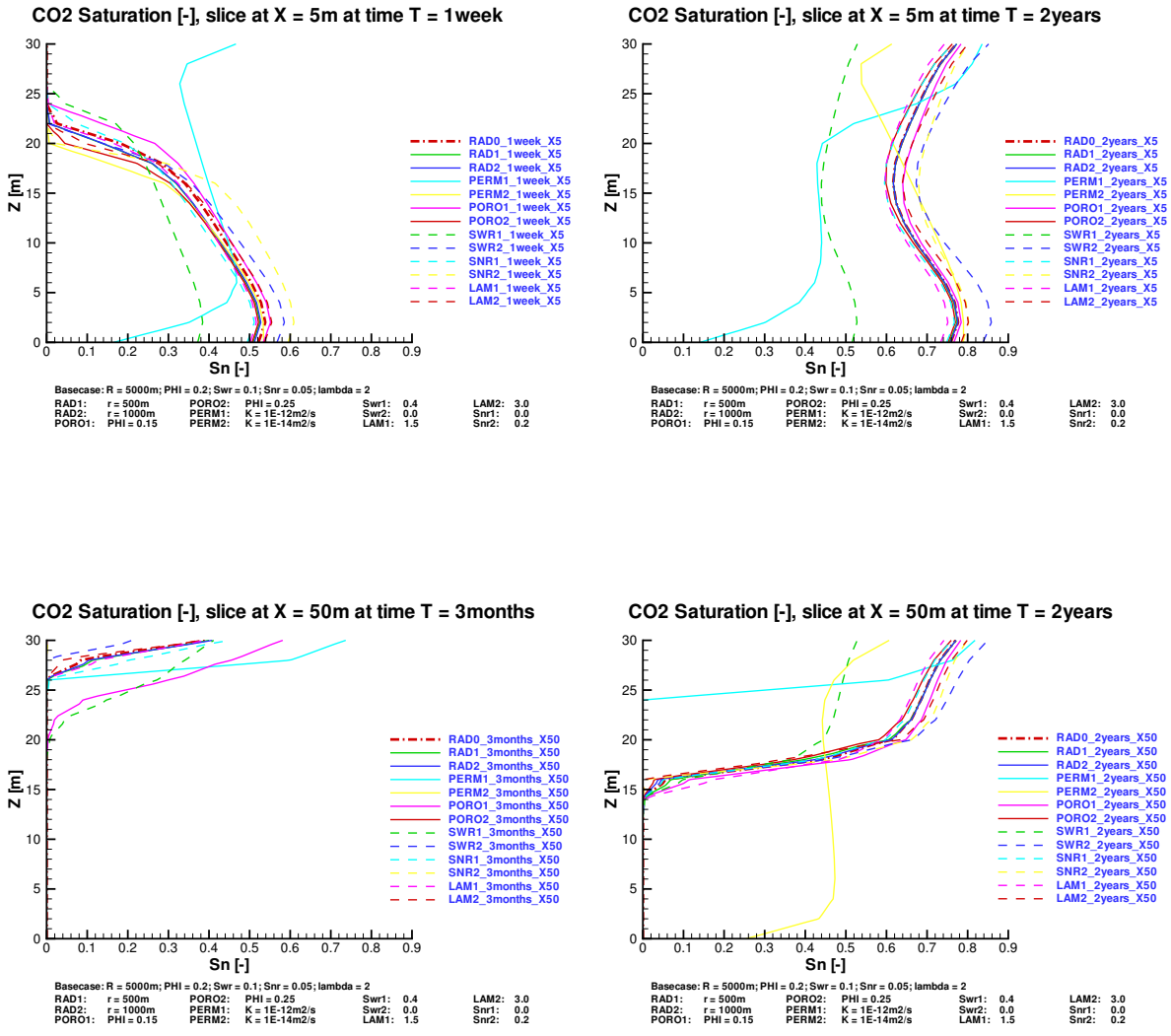

Figure 12:
Top: CO_2 saturation versus height of reservoir at a radial distance of 5 [m] to the injection well one week (left) and two years (right) after start of injection.
Bottom: CO_2 saturation versus height of reservoir at a radial distance of 50 [m] to the injection well three months (left) and two years (right) after start of injection.

Table 8: Input Parameters for the Parameter Study

Parameter	type	value	unit	comment
Salinity	X	0.2	$\frac{kg}{kg}$	$= 250\ \frac{g}{L}$
Entry Pressure	p_d	10000	Pa	
Initial conditions Water	p_w	$P_{atm} + (\varrho \cdot g \cdot h)$	bar	Hydrostatic pressure
Initial conditions CO_2	S_n	0.0	bar	Saturation = 0

a peak value of 55 [%], 2 [m] above the bottom of the reservoir (see figure 12). Buoyancy effects are not so dominant and the CO_2 forms an "orb" around the injection well, reaching a height of 23 [m]. This means the plume has not yet reached the cap-rock. After two years of continuous injection, CO_2 saturations have increased to 85 [%], also 2 [m] above the bottom of the reservoir. This is about the highest value observed in our modelling scenarios so far (for a 2 phase model). The saturation has a "S" shape, meaning that saturation increases again when approaching the cap-rock. In 50 [m] distance to the injection well three months after injection start, the saturation reaches a peak value of 38 [%] in a 4 [m] thin layer underneath the cap-rock. The CO_2 plume reaches this distance mainly driven by bouncy forces. After two years the saturation has increased to about 75 [%] and the CO_2 plume now has a thickness of 10 to 15 [m] underneath the caprock.

Cases that differ from that behaviour can now be interpreted. One can see that most of the parameter variations have an obvious impact on the saturation distribution. Some of the impact occurs later in time or at some distance to the injection well. Few of the parameters only have minor impacts. Big differences can be observed for variations in the permeability and in the residual water saturation (cases PERM1, PERM2, SWR1, SWR2).

In the PERM1 case, the higher permeability allows the buoyancy forces to take more effect. The CO_2 plume reaches the cap-rock very fast. Whereas the saturation distribution has a cylindrical shape in the beginning, it becomes very fast a thin layer underneath the caprock and reaches there the highest concentrations (almost 30 [%] after 3 months in 50 [m] distance than in the RAD0 case!).

For lower permeabilities (case PERM2), buoyancy forces are weak. The difference becomes first visible after some time of injection or in some distance. After 2 years of injection and in 5 [m] distance, the saturation at the caprock is much lower than for almost all other cases. The saturation has not increased at all at 50 [m] distance after 3 months. This can clearly be addressed to the weakened influence of the buoyancy forces. After 2 years the plume has reached the 50 [m] mark, almost over the entire depth of the reservoir with a saturation higher than 45 [%].

In the SWR1 case, the increased residual water saturation generally prevents high CO_2

saturations. The saturations are everywhere and at every time among the lowest ones. But the shape of the saturation distribution is similar to the RAD0 case. The SWR2 case, in contrast, has always slightly higher concentrations than case RAD0. This means obviously, the residual water saturation has a high influence on the maximal occurring CO_2 saturations!

The lateral extent of the reservoir in the model has almost no effect on the saturations. The 1 [km] radius reservoir is even identical to the 5 [km] radius reservoir. This means a lateral extent of 5 [km] for the reservoir is enough. Porosity (case PORO1 and PORO2) has only a minor effect on the saturation. It seems that the difference in porosity scales inverse with the difference in the saturation observed. When the porosity is lowered by 5 [%], the saturation is in average about 5 [%] higher and vice versa.

Variations in the residual gas saturation (cases SNR1 and SNR2) and in the λ value have little effect.

5.4 Pressure Evolution

The pressure evolution is shown as pressure versus time for a specific point in the reservoir. Most interesting points are located at the cap-rock in various distances to the injection well. See Figure 13 for pressure plots of points at the cap-rock just above the injection well and in 50, 100 and 500 [m] distance. The undisturbed reservoir pressure is 84.08 [bar], marked by the black dotted line.

Again, the RAD0-Case is the basis for all the interpretation. In this case, the overpressure rises to a maximum of 4.3 [bar] after 59 days. Then it declines continuosly and after 2 years of injection the overpressure has fallen to 3.2 [bar]. In 50 [m] distance the pressure rises slowly after start of injection and then, when CO_2 saturation increases rapidly, so does the gas pressure (the CO_2 concentration is 10 [%] after 80 days, then it rises to 40 [%] within 9 days, and to 50 [%] within 20 days). The rapid increase of gas pressure can be described with the help of the conceptual model. Brine pressure and CO_2 saturation are primary variables, meaning they are unknowns in our system of differential equations. Gas pressure and capillary pressure are calculated after solving for the primary variables. They are computed algebraic complementary constraints. The capillary pressure is calculated as function of the saturation (see figure 1). When the water saturation decreases, the capillary pressure increases. The gas pressure is then calculated by summing up the brine pressure and the capillary pressure. Therefore when the water saturation decreases, due to the fact that it is displaced by CO_2, the capillary pressure rises and so does the gas pressure. In this way it is possible to estimate a steep rise in saturation by looking at the gas pressure. The maximum overpressure is 3.5 [bar] after 133 days. In 100 [m] distance the maximum overpressure is only 2.8 [bar] after 238 days. The rise in pressure when the CO_2 plume arrives is after 200 days. In 500 [m] distance the maximum overpressure is even less, 1.6 [bar] and still increasing

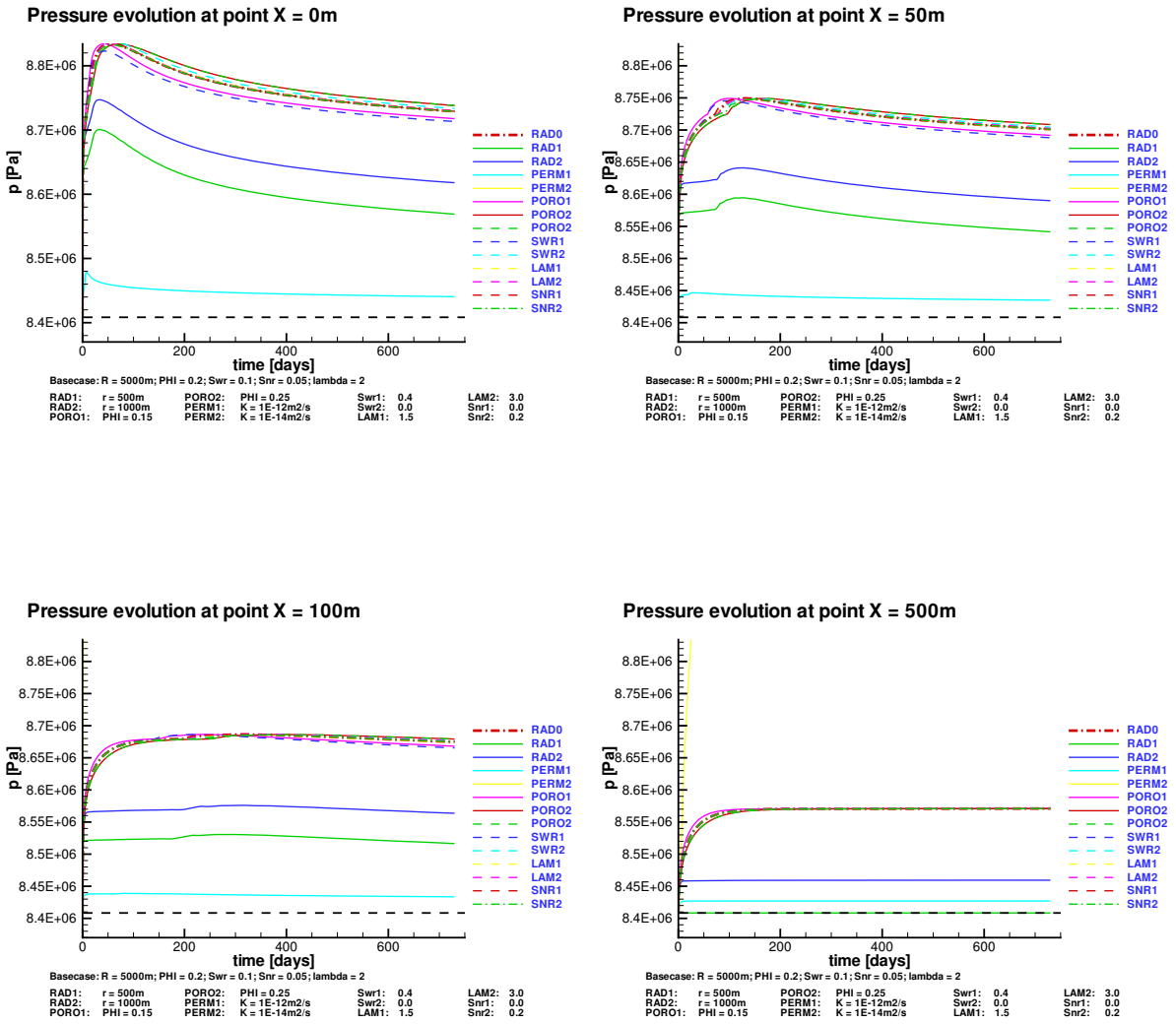

Figure 13:
Top: Gas pressure versus time after start of injection at the cap-rock above the injection well (left) and for a point in 50 [m] distance (right).
Bottom: Gas pressure versus time after start of injection at the cap-rock for a point in 100 [m] distance (left) and 500 [m] distance (right).

after 2 years of injection.
The most obvious difference from the descibed pressure evolution result from a variation in permeability, lateral extent of the domain, porosity and residual water saturation (PERM1, PERM2, RAD1, RAD2, PORO1, PORO2, SWR1 and SWR2). A lower permeability (PERM1) has higher overpressures as a result, in case of PERM2 so high that they are not visualised here (maximum overpressure is 31 [bar]). Since such a high overpressure would not be possible in Ketzin, due to a fracture pressure of around 10 [bar], the assumption of a continuous injection with a low permeability is not reasonable. A higher permeability (PERM2) results in much lower overpressures, here maximal 0.7 [bar]. The pressure peak occurs much earlier in this case, after 7 days. In contrast to the influence on the saturation evolution, the lateral extent of the domain has a high influence on the modeled overpressures. When the domain is selected to small, the overpressures are much lower. For the case of a reservoir with a 500 [m] radius, the overpressure is only half the value of a reservoir with 5000 [m] radius. We observed that a radius of 5000 [m] should be reasonable for this principle investigation. When setting up the complex reservoir model, the effects of the selected boundaries have to be investigated in detail. The porosity has a minor effect on the overpressure, but it has on the time when the peak is reached. A lower porosity results in an earlier peak overpressure. In this case, by lowering the porosity by 5 [%] the peak occurs after 40 days instead of 59 days. Increasing the porosity has the same effects, the peak occurs in case of PORO2 after 73 days. Modifying the residual water saturation has two effects. When increasing the residual water saturation (SWR1) the peak overpressure is slightly less (0.1 [bar]) and occurs earlier (10 days). When lowering the residual water saturation (SWR2), this leads to slightly higher and later peak overpressure.

6 Code Intercomparison Study

The code intercomparison study was developed to asses the reliability of the numerical models and delineate best practice procedures for similar types of projects. The issues that made this necessary are as follows:

- The codes exhibit such a degree of complexity that it is not possible to verify them against analytical solutions.
- The implemented thermodynamic database implemented may differ from code to code, so that results and the behaviour of the CO_2 may differ for the same problem.
- The discretisation and solution techniques for the differential equations differ from code to code.
- Simplifications of mathematics and physics may differ between the codes.

The **Dept. of Hydromechanics and Modeling of Hydrosystems** took already part in a code intercomparison study for CO_2 sequestration issues in 2002 (Pruess et al. (2002) [10]).

6.1 Model Domain

A radial symmetric domain is chosen to best represent the reservoir (see figure 3). In this case the lateral extent is 100 [km]. This very large model domain addresses the issue of boundary conditions unintentionaly influencing the results, when their distance to the injection well is chosen to close. This issue was also addressed in the Parameter Study (cf. section 5). The modelarea represented in this way is about 31.415 [km^2]. The smallest grid cell length is 50 [cm] at the injection well. The height of the domain is 30 [m] and the injection well diameter is 0.25 [m]. This fairly large well diameter has been selected due to numerical reasons. We simulated a very long time span of 100 [years] which takes some computation time. This computation time can be shortened when the time step length increases. But the maximum time step length is restricted by the flow velocity with respect to the element size. This means, the larger the elements, the larger is the potential maximum time step length and the shorter is the necessary computation time. The horizontal and the vertical permeability are equal (isotropic).

6.2 Boundary Conditions and Parameters

The boundary conditions are similar the the ones used in the preceeding scenarios. But since this numerical simulation utilises the two phase two component non-isothermal model,

additional definitions have to be made. See table 9 for boundary conditions. X_n^w denotes the mass fraction of CO_2 in the water phase. The well is completed only in the bottom most layer of 5 [m] thickness and CO_2 is injected in supercritical condition for 2 years time. The flux is kept constant at a value of 1 $[\frac{kg}{s}]$ (see Table 9). After the injection is stopped the CO_2 is monitored for a total time span of 100 [years]. The hydrostatic pressure refers to a depth of 760 [m] at the bottom and 730 [m] at the top of the reservoir (this is the same depth as in section 5).

Table 9: Boundary Conditions

boundary	type	value	unit	comment
top, bottom, side	NEUMANN q_w	0.0	$\frac{kg}{m^2 \cdot s}$	NO-FLOW
top, bottom, side	NEUMANN q_{CO2}	0.0	$\frac{kg}{m^2 \cdot s}$	NO-FLOW
top, bottom, side	NEUMANN q_h	0.0	$\frac{J}{s}$	NO-FLOW
lateral	DIRICHLET p_w	$P_{atm} + (\varrho \cdot g \cdot h)$	bar	HYDROSTATIC
lateral	DIRICHLET X_n^w	10^{-9}	$\frac{kg}{kg}$	MASS FRACTION
lateral	DIRICHLET T	$-\frac{z}{15} + 309.15$	K	$0 < z < 30$
injection well	NEUMANN q_w	0.0	$\frac{kg}{m^2 \cdot s}$	NO-FLOW
injection well	NEUMANN q_{CO2}	-1.0	$\frac{kg}{s}$	
injection well	DIRICHLET T	309.15	K	

For other model input parameters see table 10.

Table 10: Input Parameters code intercomparison study

Parameter	type	value	unit	comment
Permeability	K	$3 \cdot 10^{-14}$	m^2	
Porosity	ϕ	0.2	-	
Salinity	X	0.2	$\frac{kg}{kg}$	$= 250\ \frac{g}{L}$
Res. Water Sat.	S_{wr}	0.1	-	
Res. CO_2 Sat.	S_{nr}	0.05	-	
Entry Pressure	p_d	10000	Pa	
Lambda	λ	2	-	
Init. cond. Water	p_w	$P_{atm} + (\varrho \cdot g \cdot h)$	bar	Hydrostatic pressure
Init. cond. CO_2	X_n^w	10^{-9}	$\frac{kg}{kg}$	Mass fraction of CO_2 in brine
Init. cond. Temperature	T	$-\frac{z}{15} + 309.15$	K	Geothermal grad.$(0 < z < 30)$

In this study, due to numerical stability reasons the capillary pressure-saturation relation, as shown in figure 1, is modified. As soon as the water saturation is lower than the residual

water saturation ($S_w < S_{wr}$) the capillary pressure is regularised to $p_{c\,reg} = (S_{wr}\text{-}S_w) \cdot 5 \cdot 10^5$ Pa + p_c.

The solubility of CO_2 in water is calculated as a function of pressure, temperature and salinity. The solubility of water in CO_2 is set to zero.

6.3 Saturations, Pressure Evolution and Solubilities

At a lateral distance of 2 [m] to the injection well (see figure 14), 10 days after start of injection the CO_2 saturation front forms a orb around the source, not reaching the cap-rock yet. After 1 and 2 years of injection the saturation over depth has a "S" shape, reaching a saturation of 100 [%] in the lower part of the reservoir, decreases then, and increases again when coming close to the cap-rock. This high saturations of 100 [%] are possible in the 2 phase 2 component non-isothermal model concept, because here the water saturation can fall under the residual water saturation by mass-transfer of water into the CO_2 phase. After 2 years the injection of supercritical CO_2 stops. Buoyancy forcs drive the CO_2 plume upwards. The lowest saturations are 0.05 in the lower region of the reservoir, which is the residual saturation.
Brine overpressure increases to about 9 to 12 [bar] after 10 days. It slightly keeps increasing within the injecting 2 years period. Then the pressure falls back to hydrostatic pressure. The CO_2 dissolved in brine reaches almost immediately 13 $[\frac{sm^3_{CO_2}}{sm^3_{brine}}]$ and stays at this value for the entire time span considered. After 10 days, only in the uppermost region of the reservoir the dissolved CO_2 is lower.

The plots for CO_2 saturation, brine pressure and dissolved CO_2 in 10 [m] distance (see figure 15) to the injection well look very similar to those in 2 [m] distance. CO_2 saturation after 10 days is slightly less, but the function has the same shape. The plots for 1 and 2 years after injection start, have much lower saturations in the lower part of the domain. They do only reach between 60 and 80 [%]. CO_2 saturations for later points in time are identical. Brine pressure is identical, except the slightly lower pressure after 10 days and the missing pressure decrease in the lower part of the domain. Amount of dissolved CO_2 is only different for 10 days. Here the amount of dissolved CO_2 is lower in the middle part of the domain.

At a lateral distance of 100 [m] to the injection well (see figure 16), CO_2 can only be found underneath the cap-rock and only after 2 years and later. The saturation maximum is 80 [%] at the cap-rock. Brine pressure is from hydrostatic pressure increased by a constant value of 4 [bar] for 10 days, 11 [bar] for 1 year and 12 [bar] for 2 years after injection start. Then brine pressure normalises to hydrostatic pressure again. The amount of CO_2 dissolved in brine is zero in the 10 days and 1 years plot. After that the amount of dissolved CO_2 increases towards the cap-rock to 13 $[\frac{sm^3_{CO_2}}{sm^3_{brine}}]$.

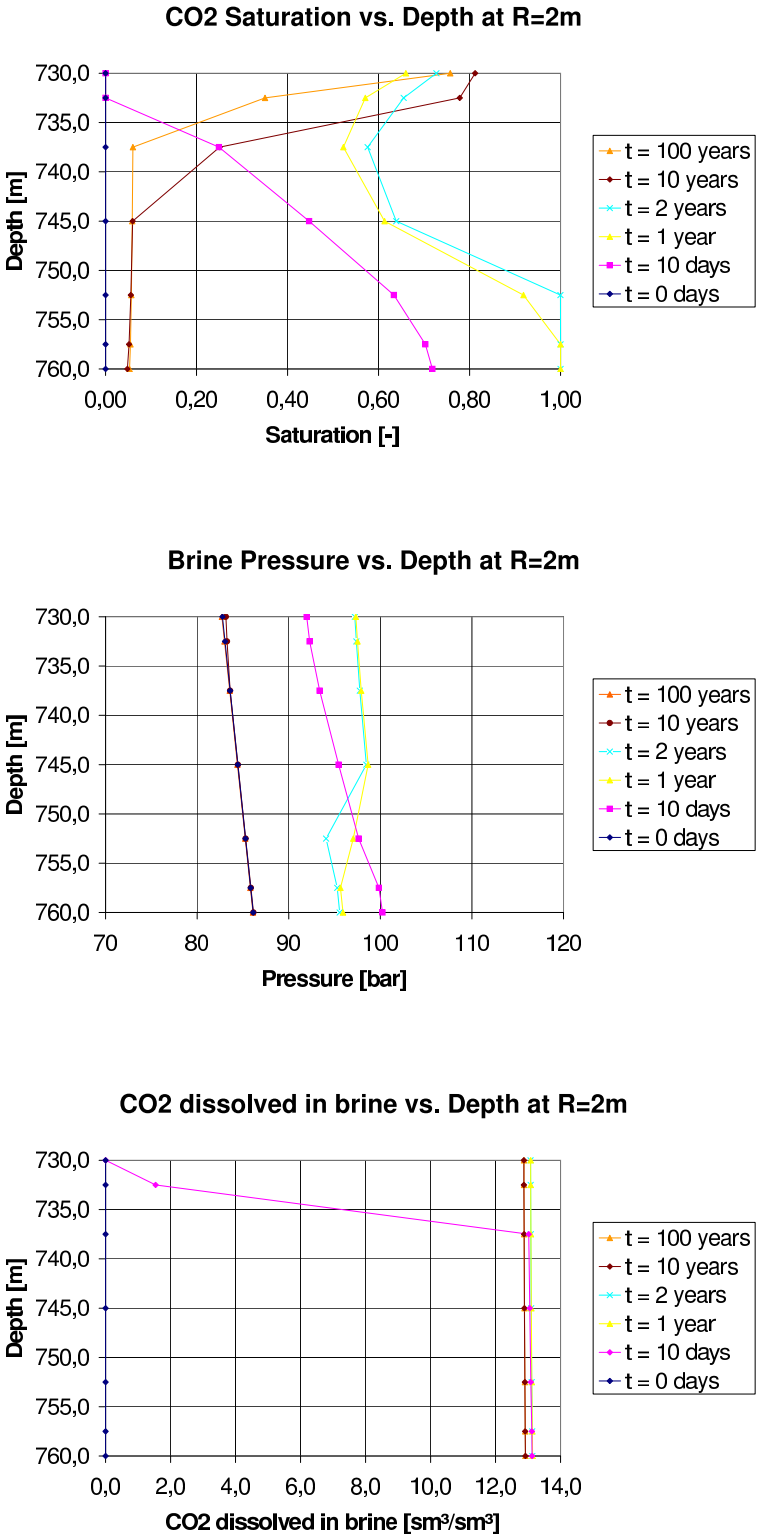

Figure 14: CO_2 Saturation (top), brine pressure (middle) and dissolved CO_2 (bottom) vs. depth in 2 [m] radial distance to the injection well.

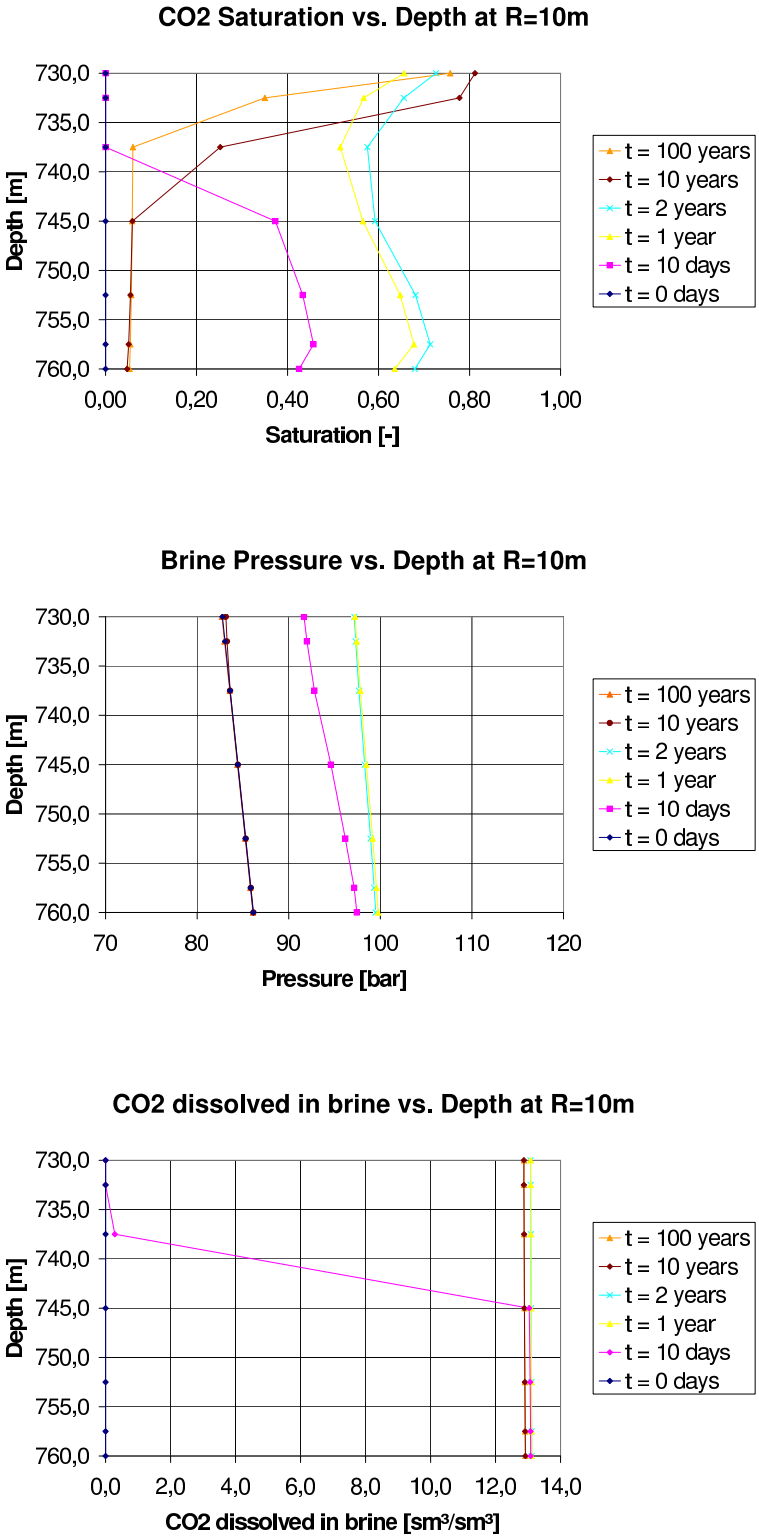

Figure 15: CO_2 Saturation (top), brine pressure (middle) and dissolved CO_2 (bottom) vs. depth in 10 [m] radial distance to the injection well.

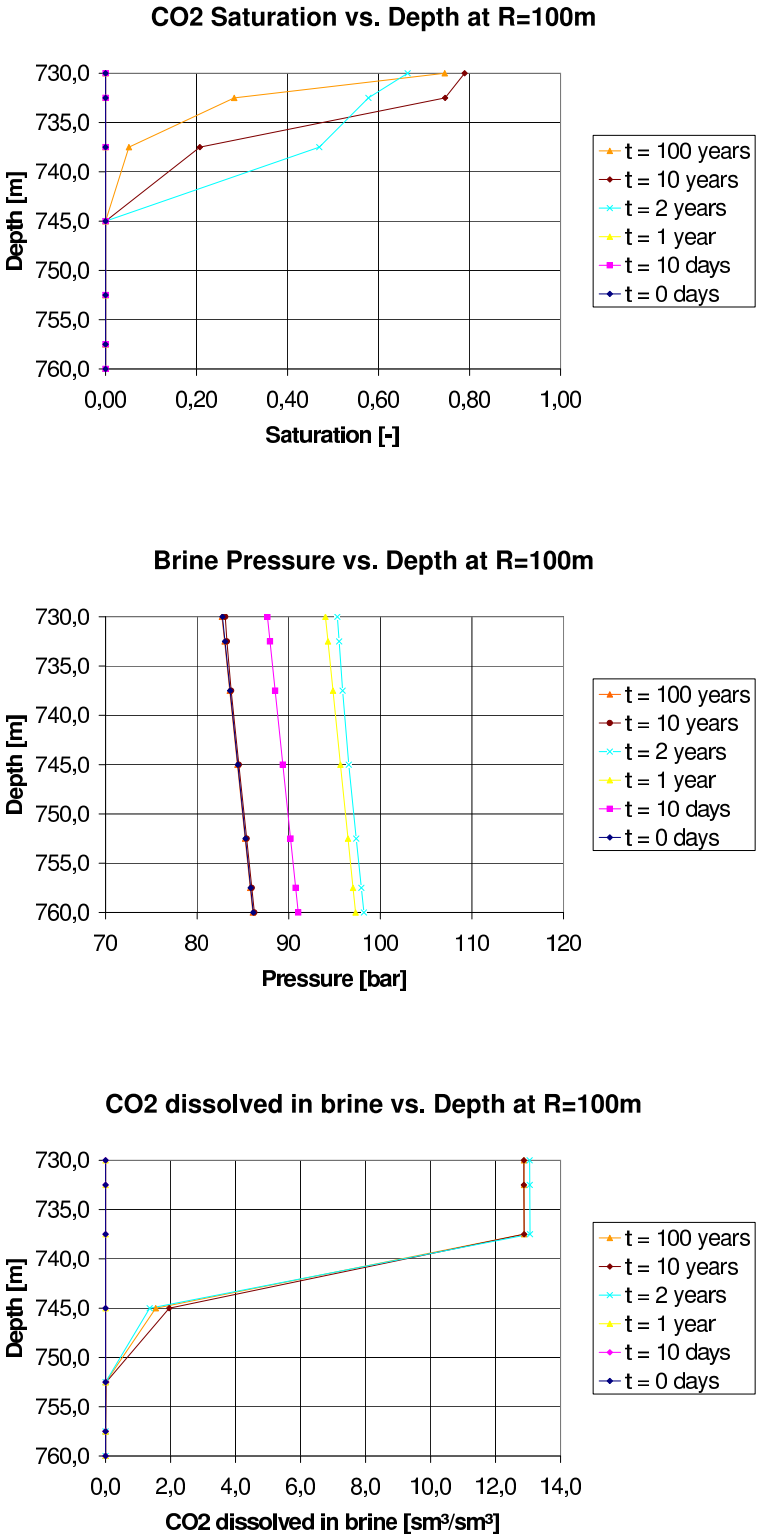

Figure 16: CO_2 Saturation (top), brine pressure (middle) and dissolved CO_2 (bottom) vs. depth in 100 [m] radial distance to the injection well.

7 Summary and outlook

In Section 3 the conceptual model is explained. It shows how relative permeability-saturation relation, capillary pressure-saturation relation and fluid and matrix properties are represented in the modell.

In Section 4 the geological model by SCRF is used to represent absolute permeability and porosity in a numerical model to estimate the arrival time, injected mass and volume of the CO_2 plume at some defined observation wells. This supports the planning, positioning and the layout of the injection and the observation wells. For the positioning of the observation wells in relation to the injection well, it is important to have such estimates of the arrival times of the 10% and 60% saturation fronts for the seismic wave detection.

In Section 5 the issue of parameter uncertainty is addressed. The parameter information about the Stuttgart Formation in Ketzin are very sparse up till now. The study gave valuable insight about the influence of the parameters to the highly nonlinear system of coupled differential equations used to describe the multiphase flow regime of CO_2 injection into the subsurface. The model was set up with Ketzin like characteristics. Starting from this parameter values, the most important parameters have been varied. Then, the results of pressure evolution and saturation distribution were compared with the original case and discussed. Parameters that have been investigated were the radial extent of the model domain, absolute permeability, porosity, residual water saturation, residual gas saturation and λ (λ describes the pore scale homogeneity of the reservoir).

In Section 6 a code intercomparison study was conducted to asses the reliability of the numerical model and delineate best practice procedures for similar types of projects. The issues that made this investigation necessary include a high degree of code complexity, possible differences in the implemented thermodynamic databases, different discretisation and solution techniques for the differential equations and simplifications of mathematics and physics may differ between the codes.

Next steps include the integration of the geological model in it's full complexity, meaning the geostatistical permeability and porosity distribution. Actually we further improve grid generation techniques to include the assumed shape of the anticline. Additional information by other groups will be integrated. Especially the integration of knowledge gained by the borehole drilling (cores, laboratory testing etc.) is of high interest. Reccomendations for parameters of high interest for us are made in section **??**. With this updated numerical model, complex injection scenarios will be conducted.

8 Cooperation and contact

This work is a close cooperation between the above mentioned authors and the following project partners:

Suzanne Hurter	(Shell)
Kim Zink-Jorgensen	(GEUS)
Niels Bech	(GEUS)
Ben Norden	(GFZ)
Hartmut Schütt	(GFZ)
Björn Legarth	(GFZ)

We are always happy to receive your questions, comments, and remarks on this work, so please do not hesitate to contact us:

andreas.bielinski@iws.uni-stuttgart.de	+49/(0)711/685-4667
andreas.kopp@iws.uni-stuttgart.de	+49/(0)711/685-4736

References

[1] Class, H. and Helmig, R. Numerical simulation of non–isothermal multiphase multicomponent processes in porous media. - 2. Applications for the injection of steam and air. *Adv. Water Resour.*, 25:551–564, 2002.

[2] Class, H., Helmig, R., and Bastian, P. Numerical simulation of non–isothermal multiphase multicomponent processes in porous media. - 1. An efficient solution technique. *Adv. Water Resour.*, 25:533–550, 2002.

[3] Deutsch, C. and Journel, A. *GSLIB - Geostatistical Software Library and Users Giude: 2nd edition* . Oxford University Press, 2002.

[4] Deutsch, C. and Tran, T. A program for object-based stochastic modelling of fluvial depositional systems . *Computers and Geosciences*, 28(3):252–535, 2002.

[5] Deutsch, C. and Wang, L. Hierachical object-based stochastic modelling of fluvial reservoirs. *Mathematical Geology*, 28(7):857–880, 1996.

[6] Helmig, R., Class, H., Huber, R., Sheta, H., Ewing, R., Hinkelmann, R., Jakobs, H., and Bastian, P. Architecture of the Modular Program System MUFTE_UG for Simulating Multiphase Flow and Transport Processes in Heterogeneous Porous Media. *Mathematische Geologie*, 2:123–131, 1998.

[7] Helmig, R. *Multiphase Flow and Transport Processes in the Subsurface*. Springer, 1997.

[8] Kretzschmar, H.-J., Bittkow, P., and Haeusser, D. Gas-Wasser-Verdrängungsmodell für Aquiferspeicher, Teil II, Reservoirmechanisch-petrophysikalische Speichereigenschaften Lias alpha des UGS Ketzin. Research report, Brennstoffinstitut Freiberg, Forschungsgruppe Verfahrenstechnik UGS, 1972.

[9] Kretzschmar, H.-J., Bittkow, P., Haeusser, D., and Hanne, G. Studie Schilfsandstein. Research report, Brennstoffinstitut Freiberg, Forschungsgruppe Verfahrenstechnik UGS, 1973.

[10] Pruess, K., Bielinski, A., Ennis-King, J., Fabriol, R., Le Gallo, Y., Garcia, J., Jessen, K., Kovscek, T., Law, D.-S., Lichtner, P., Oldenburg, C., Pawar, R., Rutqvist, J., Steefel, C., Travis, B., Tsang, C.-F., White, S., and Xu, T. Code Intercomparison Builds Confidence in Numerical Models for Geologic Disposal of CO2. In *Gale, J. and Kaya, Y. (Editors): GHGT-6 Conference Proceedings: Greenhouse Gas Control Technologies*, S. 463–470, 2003.